

YBa₂Cu₃O_{7-δ}-Based, Edge-Geometry SNS Josephson Junctions with Low-resistivity PrBa₂Cu₃O_{7-δ} Barriers

J. B. Barrier, B. D. Hunt, M. C. Foote, W. T. Pike, and R. P. Vasquez.

Center for Space Microelectronics Technology

Jet Propulsion Laboratory

California Institute of Technology

4800 Oak Grove Drive

Pasadena, CA 91109-8099

Abstract

We investigated the properties of all-high-T_c edge-geometry Josephson weak links using superconducting YBa₂Cu₃O_{7-δ} (YBCO) electrodes and PrBa₂Cu₃O_{7-δ} (PBCO) normal-metal layers. The fabrication of the weak-links involved first ion-milling the base YBCO film using a MgO mask to form the edge and then depositing PBCO and YBCO layers in situ by pulsed-laser deposition. The optimum PBCO films had resistivities of 2 to 4 mΩ cm at room temperature and ~30 mΩ cm at 4.2 K. Current-versus-voltage (I-V) characteristics were qualitatively consistent with the resistively-shunted-junction (RSJ) model. Strong Shapiro steps were present in the I-V characteristics of junctions under microwave irradiation and the critical current of the devices modulated with a Fraunhofer-like dependence as a function of magnetic field. The device parameters exhibited good scaling with area and PBCO thickness. The critical-current density varied exponentially with PBCO thickness, yielding a normal-metal coherence length of 9 nm for the PBCO.

Keywords: Superconductivity, Josephson Junction, PrBa₂Cu₃O_{7-δ}, YBa₂Cu₃O_{7-δ} weak-link.

Introduction

The future of high-transition-temperature (T_c) superconductive electronics depends on finding solutions to many technological issues in thin-film growth and device fabrication. At the heart of these problems is the lack of reliability and reproducibility in the fabrication of Josephson junctions. To date, there has not been a method of fabricating all high- T_c superconductor/insulator/superconductor (SIS) structures. Therefore, the majority of work has focused on the fabrication of superconductor/normal-metal/superconductor (SNS) Josephson junctions, or weak links with electrical performance consistent with the resistively-shunted-junction (RSJ) model. [1]

The methods of fabricating SNS-like devices fall into two basic categories. The first category stems from the fact that suppression of the superconducting order parameter occurs in or near grain boundaries in the high- T_c oxides and this acts to disrupt the superconducting properties near the grain boundary on the scale of the coherence length. Thus, a weak-link Josephson junction can be fabricated by isolating small areas of the electrodes near the grain boundary. Such approaches include the use of naturally occurring grain-boundaries, [2,3] grain boundaries formed on a step edge [4] and grain boundaries formed on hetero-crystal interfaces [5] or bi-epitaxial interfaces. [6]

Although the use of grain boundaries has produced some of the best high- T_c Josephson devices to date, this method does not generally afford flexibility, reliability and control of the device parameters. The control of the device parameters is of particular interest to circuit design and fabrication where control of the device resistance and critical current is necessary, often over a wide range.

To this end, many groups have focused on the fabrication of SNS devices using superconductive oxide electrodes and deposited normal-metal layers of varying thicknesses to control the device parameters. The work in this area has involved the use of noble metals [7- 10] and a variety of oxides. The latter include $\text{PrBa}_2\text{Cu}_3\text{O}_{7-\delta}$ (PBCO), [11-15] normal $\text{YBa}_2\text{Cu}_3\text{O}_{7-\delta}$, [16] Nb-doped [17] and undoped SrTiO_3 , [18] $\text{La}_{1.5}\text{Ba}_{1.5}\text{Cu}_3\text{O}_{7-y}$, [19] $\text{La}_{0.7}\text{Ca}_{0.3}\text{MnO}_2$, [20] $\text{Bi}_2\text{Sr}_2(\text{Ca}, \text{Bi}, \text{Sr}, \text{Dy})_{n-1}\text{Cu}_n\text{O}_{2n+4}$, [21] MgO , [22] and CaRuO_3 . [23] These oxides show particular promise because of the close lattice match and growth conditions with respect to their corresponding oxide superconductors. More importantly, most of the work with these normal oxide materials has shown some initial success in that the devices' characteristics were qualitatively consistent with predictions of the RSJ model.

In this paper we report on our work using low-resistivity PBCO thin films as the normal layers in all-high- T_c , epitaxial, edge-geometry SNS Josephson junctions employing $\text{YBa}_2\text{Cu}_3\text{O}_{7-\delta}$ (YBCO) electrodes. We have been able to produce by pulsed-laser ablation thin films of PBCO with significantly lower resistivity than previously reported for bulk polycrystalline PBCO [24] and other device-related work. [13- 15] While the exact origin of the lower resistivity is unknown, it is more consistent with single crystal material [24] and the device work carried out by Rogers, et al., [11] and Barrier, et al. [12]

Devices fabricated with this lower resistivity PBCO exhibit current-voltage (I-V) characteristics qualitatively consistent with the RSJ model. The devices exhibit well-defined ac and dc Josephson effects. The critical-current density depends exponentially on PBCO thickness and this dependence yields a normal coherence length of 9 nm. We observe good areal scaling for the device parameters. The device resistance depends linearly on PBCO thickness and the derived

resistivity from the devices is consistent with the value measured from individual films of PBCO.

Many of our observations are consistent with “classical” proximity-effect induced superconductivity in the PBCO layer. The devices begin to exhibit a supercurrent at a temperature which decreases by increasing the PBCO film thickness. Furthermore, the critical current depends exponentially on temperature at low temperatures for sufficiently thick PBCO barriers.

Device Fabrication and Material Properties

The fabrication process of our epitaxial all-high- T_c edge-geometry Josephson device was described in detail elsewhere.[16] Represented in figure 1 is our device geometry. We will only review the basic processing steps here.

We first deposited c-axis oriented YBCO films on (100) LaAlO_3 substrates by pulsed-laser ablation of a YBCO target. The substrate temperature was typically ~ 825 C, as measured by a pyrometer using highly doped Si chips mounted next to the device samples. The oxygen pressure was approximately 100-120 mTorr. The thickness of the YBCO films ranged from 200 to 250 nm and the growth rate was ~ 0.1 nm/sec. After a standard oxygen (100 Torr) anneal and cooling the substrate to ≤ 200 C, we deposited of a 10 nm-thick MgO passivation film on the YBCO by RF magnetron sputtering. Patterning of a photoresist lift-off stencil followed by the deposition of a 0.6 to 0.8 μm -thick MgO film by electron-beam evaporation served to form the ion-milling mask after completion of the lift-off process. Ion-milling of the edge was done with 500 eV Ar ions at a current density of ~ 1 mA/cm². During this edge-cutting step, the position of the substrate was at a 60° angle from normal incidence of the ion beam, which resulted in formation of a shallow, tapered edge in

the YBCO base electrode. [16] The angled edge was intended to prevent grain boundary formation during growth of the subsequent layers on the edge. [4] The sample was then rotated in dry high-purity nitrogen to an angle of normal incidence for a 2 minute, low-energy (50 eV, $\sim 0.1 \text{ A/cm}^2$) ion-mill clean.

Following the ion-mill clean, the sample was transferred in situ to the pulsed-laser ablation growth area of our system for growth of the PBCO N-layer and YBCO counterelectrode film. Thus, the entire process from cutting the edge to growth of the N-layer and counterelectrode YBCO was performed completely in situ or in an inert atmosphere. For the work presented in this paper, the growth conditions for the PBCO films were the same conditions as for the YBCO films. Individual devices were patterned by ion milling using standard photoresist milling masks and lithographic processes. The devices had widths varying from 6 to $1.5 \mu\text{m}$ and, hence, effective areas ranging from 3×10^{-8} to $7.5 \times 10^{-9} \text{ cm}^2$. Each sample, or chip, contained eight devices with tapered edges (-600), two devices with steeper edges (-450), base-electrode and counterelectrode current-density bridges, and a set of assorted dc SQUID's as well as an area devoted to material characterization. All the devices and SQUID's were contacted with Au bonding pads. For the studies presented here, we fabricated devices with PBCO thicknesses of 10, 20, 30 and 50 nm. There were two chips at each PBCO thickness.

The material properties of our pulsed-laser deposited PBCO films were studied. These studies were undertaken on films directly deposited onto bare LaAlO_3 substrates and not on a YBCO film or a device edge. The x-ray diffraction data taken from these films revealed that they are c-axis oriented with a c-axis lattice parameter of 1.172 nm, which agrees with results obtained from powder x-ray diffraction of fully oxygenated PBCO. [24] However, there were a few unidentified small peaks. No peaks were found which could be associated with a-

or b-axis growth and the size of the c-axis lattice parameter suggests that the crystalline state of the films is orthorhombic.

Figure 2 shows a cross-sectional transmission electron micrograph (XTEM) of a PBCO/YBCO/Au trilayer. Deposition of the trilayer was during the device processing step wherein the edge was defined and the N-layer, superconducting counterelectrode and contact metal were deposited. The nominal thicknesses of the films were 50, 200, and 30 nm for the PBCO, YBCO and Au, respectively. While the XTEM does not show an active device edge, it does reveal a number of important observations that will help to understand the microscopic structure of our devices.

The XTEM in figure 2 shows clear c-axis orientation of the PBCO and YBCO layers as manifested by the CU-O planes. The Z-contrast between Pr and Y is similar so clear determination of the interface is difficult. However, careful inspection of the micrograph reveals a basic thickness modulation in the PBCO layer that propagates through the subsequent layers. This thickness variation is ~ 6 nm. There are no pinholes visible within the limited field of view of the micrograph. Indeed, we have examined about $10\text{ }\mu\text{m}$ in length of the cross-sectioned sample and found no pinholes. However, these observations do not rule out the existence of pinholes in the actual device layers fabricated on a tapered YBCO edge.

Electrical Properties

We begin the presentation of the electrical properties of our YBCO/PBCO/YBCO edge-geometry devices by discussing the conduction properties of the PBCO. The resistivity-versus-temperature data of a PBCO film on LaAlO_3 is

presented in figure 3. The current (I) and voltage (V) contacts were placed on the film as shown in the inset. The resistivity-versus-temperature data has an overall character qualitatively similar to that observed previously. [24] The resistivity of our PBCO films is observed to increase with decreasing temperature from room temperature to liquid helium temperature. This temperature dependence of the resistivity suggests thermally activated carriers and/or a variable-range hopping mechanism through localized states. The data in figure 3 could not be fit to a single activation energy and this is similar to the results of Fisher, et al. [25] However, the resistivity is at least 1 order of magnitude lower than previously reported bulk or polycrystalline results [24] for all temperatures and many orders of magnitude smaller at low temperatures.

The origin of the lower resistivity for our PBCO films is unclear. It has been shown that the resistivity of single crystals of $\text{Y}_{1-x}\text{Pr}_x\text{Ba}_2\text{Cu}_3\text{O}_{7-\delta}$ can be orders of magnitude lower than polycrystalline bulk material [24] and similar results might be expected for our highly oriented films. In addition, we note that there was a set of small, unidentified peaks in the x-ray diffraction spectra that could lead to the lower resistivity. However, no evidence of impurities was observed in the cross-sectional transmission electron micrographs and the peaks observed in x-ray diffraction data are indicative of a very small fraction of the sample. Additionally, it has been shown that the resistivity of the PBCO can be lowered by annealing in oxygen at higher than normal temperatures. [26] Our films were deposited and annealed in oxygen at growth temperatures ($\sim 825^\circ\text{C}$) considerably higher than used in some of the previous device experiments. [13- 15] These higher temperatures may lead to lower resistivities in this work as well as in some of the other device work [11, 12] with PBCO barriers.

We have measured the resistance of our YBCO/PBCO/YBCO devices from room temperature to below their critical temperatures. In figure 4, we show the results of these measurements for a representative set of devices with different PBCO thicknesses. The measurement was performed with a lock-in amplifier and a peak-to-peak drive current less than $1\text{ }\mu\text{A}$ was used to obtain each of the curves.

Above 100 K, the devices exhibit a linear resistance-versus-temperature curve associated with electrical transport through the YBCO electrodes. Below 100 K, the devices exhibit a large drop in resistance at temperatures between 85 and 88 K that is consistent with the electrode transition temperatures measured for these device chips. There was no correlation between the electrode transition temperatures and thicknesses of the PBCO layers in the devices.

We want to focus on the behavior of our devices below the electrode transition temperatures ($< 85\text{ K}$). Interestingly, a “foot” develops in the resistance-versus-temperature curves as the PBCO thickness is increased. The device transition temperatures are -70 , 57 and 27 K for PBCO thicknesses of 10 , 20 and 30 nm , respectively. We observed some variation in this transition temperature from device to device of about 5 K . We also fabricated junctions with 50 nm -thick PBCO layers which showed no supercurrent down to 4.2 K .

A theory for the origin of the foot in the resistance-versus-temperature data in grain-boundary junctions has been proposed by Gross, et al. [27] In their model, the foot arises from thermally activated phase slippage (TAPS) across the Josephson junction. Gao, et al. [13] used this model to explain their data obtained from YBCO/PBCO/YBCO edge-geometry junctions. We have examined our data within the framework of the TAPS model. Reasonable fits to the data could be obtained, but only for a limited temperature range just above T_c^{dev} of the device.

Here, T_c^{dev} of the device is defined as the temperature when the device begins to exhibit a non-zero supercurrent. The temperature range where the data could be fit to the TAPS model corresponds to resistances < 0.2 to 0.4Ω in figure 4. For example, the temperature range would be from $T_c^{\text{dev}} = 27$ to ~ 34 K in case of the junction with a 30 nm-thick PBCO layer. Within this limited temperature range the TAPS model may be used to explain our data.

In contrast to other reported device work, [13,27] the data could not be fit to the TAPS model over the temperature range from a few degrees above T_c^{dev} to the electrode T_c (-85 K). This temperature range is from -34 K to -85 K, ~ 63 to -85 K, and ~ 75 to 85 K for PBCO thicknesses of 30, 20 and 10 nm, respectively. We note that for each PBCO thickness, the resistance decreases exponentially with decreasing temperature in the range where the TAPS model does not fit the data. The failure of this model to explain our data in this temperature regime maybe due to many factors. One possibility is that TAPS does not take into account a temperature-dependent normal-layer coherence length. Furthermore, the model does not take into account the temperature dependence of the resistivity and, therefore, does not account for the temperature dependence of the mean-free path. It is obvious from the results presented in figure 3 that both of these quantities are indeed very temperature dependent assuming even the simplest conduction models for the PBCO. Nevertheless, the size of the foot is strongly dependent on the PBCO thickness and one possibility is that some aspects of the data maybe explained by a “classical” proximity-effect coupling of the two YBCO electrodes through the PBCO film. In such a framework, the foot may arise from a temperature-dependent coupling of the superconducting order parameters for each electrode through the PBCO normal layer. Further modeling will be necessary to understand our data.

We now turn our focus to the electrical properties of our YBCO/PBCO/YBCO edge-geometry junctions in the superconducting, or Josephson state at temperatures below T_c^{dev} . In figure 5, we show a typical I-V characteristic for a device with a 10 nm-thick PBCO layer. The data were taken at 65 K. The device had a normal-state resistance (R_n) of 0.65Ω and the critical current (I_c) was $400 \mu\text{A}$. The value of R_n was taken from the slope of the I-V curve above I_c at sufficiently high voltages to be in the linear portion of the I-V characteristic. The normal-state resistance and area product ($R_n A$) was $0.98 \Omega \mu\text{m}^2$. At this temperature, the $I_c R_n$ product was $260 \mu\text{V}$, which rose to 1.8 mV at 4.2 K . The latter is typical of our devices with thin PBCO normal layers and we note that the values of the $I_c R_n$ products decrease exponentially with increasing PBCO thickness.

As can be seen in figure 5, the I-V curvature is qualitatively consistent with the RSJ model[1] and we observe this type of curvature in the I-V characteristics in nearly all of our junctions with PBCO barriers. We typically observe the I-V curvature become progressively piece-wise linear and sometimes flux-flow in nature as the temperature is decreased much less than T_c^a . This may be understood in terms of self-shielding when the current density becomes large at low temperatures. In this regard, we note that the RSJ-like character of the I-V curves become less sensitive to temperature as the PBCO thickness is increased, i.e., the current density is decreased.

The presence of well-defined Shapiro steps in the I-V characteristic while the device is exposed to microwave irradiation is an important verification of the ac Josephson effect. We show the results of this test in figure 6, obtained from the same device shown in the previous figure. The data were taken at 65 K and the junction was irradiated with microwaves at a frequency of 10.5 GHz . We note that

all the step heights present in the I-V curve do modulate to zero as a function of applied microwave power, as predicted by the RSJ model for SNS devices with low capacitance.

A more important test of our YBCO/PBCO/YBCO edge-geometry devices is the response of the device critical current to an applied magnetic field, or $I_c(B)$. Figure 7 shows the results of this test at a temperature of 68 K. The measurement was performed with the field applied parallel to the direction of the current flow and substrate, as shown in figure 1. The thickness of the PBCO was 10 nm. Also shown in the figure is the expected Fraunhofer, $\sin(x)/x$, response for an ideal, rectangular, uniform current-density Josephson junction. Clearly the magnetic field dependence of I_c is qualitatively similar to the case expected for an ideal junction. However, there are two distinct differences. First, the critical current does not modulate completely to zero. Second, the calculated period—the calculation is shown inset on the figure—is longer than that observed.

The fact that I_c does not modulate to zero implies that the current density is not constant over the effective area of the junction. [28] We do note, however, that the critical current does modulate by 85% implying that a few imperfections do *not* dominate the conductivity through the PBCO layer. There are several factors that could contribute to the incomplete modulation. In the XTEM data, a thickness variation was observed in our films, particularly in the PBCO layers, and this could lead to a non-uniform current-density distribution in our devices. We also observe that the depth of the critical-current modulation decreases with decreasing temperature. This could imply that these devices are not completely in the small junction regime and that some self-shielding effects play a role. Finally, we can not rule out the possibility that the junctions are composed of a very fine-density, parallel array of microconstrictions. This scenario would require that the

distribution of the critical currents and resistances for the microconstriction ensemble be strongly peaked near the average we observe for the junction as a whole. In addition, this model may imply that the microconstrictions have a temperature dependence such that they dominate the conduction through the PBCO layers at low temperatures. However, it would be extremely difficult to use such a scheme to explain the PBCO thickness dependence on the device parameters presented later in this paper. Therefore, we believe that the principle reason for the incomplete modulation is due to the thickness variations observed in the PBCO layer.

The measured period from the $I_c(B)$ data is ~ 8 Gauss and the calculated period is 14 Gauss assuming a zero-temperature penetration depth of 200 nm. This difference implies that the effective area is larger than the fabricated area or that the penetration depth is larger. This result is similar to what we have observed for junctions with a normal YBCO barrier.[16] In addition, we can not rule out the possibility of flux-focusing effects.[29] Importantly, the larger area implies that the junction is not dominated by a few, smaller area devices in parallel.

The electrical properties of our YBCO/PBCO/YBCO edge-geometry devices show clear evidence of ac and dc Josephson effects, indicating that they are indeed Josephson junctions. However, it is important for any electronic circuit application using high- T_c materials to clarify the reproducibility and control of the junction parameters. To this end, we have examined the critical currents and resistances of the devices across a particular chip. Figure 8 shows the critical current and inverse resistance plotted as a function of device area. The PBCO thickness was 10 nm and the measurements were taken at 4.2 K. Reasonable areal scaling for these parameters is observed. Note the linear scale that clearly shows that I_c and R_n^{-1} are indeed directly proportional to the area of the devices. However, linear fits forced

to go through the origin—to the data indicate that there are a small, positive area intercepts. This may imply that the electrically active areas were smaller than the nominal physical areas. There is also some scatter in the device parameters ($\pm 15\%$) which is probably too large for integrated circuit applications. At least some of the scatter may be due to inhomogeneities in the PBCO layer and further work is necessary to produce more uniform layering.

We have also examined the dependence of the current density and resistance on the PBCO thickness. Figures 9 and figure 10 show the critical-current density (J_c) and $R_n A$ product, respectively, plotted as a function of PBCO thickness. The data plotted here were obtained from two chips, processed in parallel, at each respective thickness and all the data were taken at 4.2 K.

The current density is expected to depend exponentially on the normal-metal length for SNS devices. [1] This dependence is indeed observed in figure 9 for our edge-geometry devices with PBCO barriers. A coherence length of 9 nm was estimated from the exponential decay. This value is somewhat longer than that observed for higher resistivity PBCO barriers[13, 14] but consistent with other results [12] in which the resistivity was lower. Furthermore, a zero-thickness current density of $5 \times 10^6 \text{ A/cm}^2$ was obtained from the fit to the data. We have performed experiments in which no barrier was deposited, but with a slightly different edge-cutting and cleaning procedure. The fitted zero-thickness value is reasonably consistent with those results.

There is scatter in the data in figure 9 as was the case in the results across a single chip (Fig. 8). The standard deviation in the data presented in figure 9 is 42, 40 and 44 % of the average value at PBCO thicknesses of 10, 20 and 30 nm, respectively. The total percentage deviation is obviously somewhat larger.

Presumably much of the scatter arises from problems with control of the PBCO thickness. Nevertheless, we demonstrated good overall control of the current-density over ~ 3 orders of magnitude in J_c .

The device resistances, which are shown in figure 10, typically show more scatter than the current densities. The $R_n A$ product should depend linearly on the PBCO thickness. This dependence is observed but there is significant scatter present in the data. The fit to a linear response gives a slope of $30 \text{ m}\Omega \text{ cm}$ and a positive thickness intercept of $\sim 8 \text{ nm}$. This slope maybe taken as an average value of the resistivity for the PBCO as determined from the devices. Indeed, the value determined here is very close to the results of transport measurements (see Fig. 3) through individual films of PBCO at 4.2 K.

It is also interesting to note that the thickness intercept is approximately equal to the thickness variations observed in XTEM (Fig. 2). However, this result may be fortuitous since the XTEM was not performed on the active area, or edge in the device. If the results shown in figure 2 are representative of the thickness variation of PBCO in the active device region, then one would expect pinholes to be present in the PBCO layer as its thickness is reduced below $\sim 6 \text{ nm}$. This thickness variation would also effectively lead to an overall appearance of a thinner barrier than the average deposited barrier thickness, since the thinner regions of the PBCO barrier layer would dominate the electrical behavior of the barrier. The intercept observed in figure 10 would then be expected.

Finally, we discuss preliminary results on the temperature dependence of the critical current of these devices. As expected for SNS devices, [1] the critical current varies as $(1 - T/T_c^{\text{dev}})^2$ for temperatures near T_c^{dev} in all devices examined to date, independent of PBCO thickness. At low temperatures ($T \ll T_c^{\text{dev}}$), there is a

functional dependence of the I_t -versus-temperature data that depends on PBCO barrier thickness. The devices with 10 nm-thick barriers have approximately a linear increase in critical current with decreasing temperature. In contrast, the devices with 20 nm-thick barriers exhibit an exponential increase of the critical current as the temperature is decreased. This is expected from “classical” proximity-effect theory [1] for SNS devices when the bridge length is greater than the coherence length and the temperature is small compared to the transition temperature of the electrodes. Fits to the data in this regime yield a coherence length of 11 nm, which is consistent with the critical-current-versus-thickness results.

Conclusions

We have demonstrated that high-quality SNS edge-geometry Josephson devices can be fabricated using a low-resistivity PBCO normal layer. The PBCO films were found to have resistivities at least an order of magnitude lower than commonly found in bulk or polycrystalline material. XTEM showed that we could uniformly layer the YBCO and PBCO films which were individually continuous but each with thickness variations. The SNS devices exhibit strong ac and dc Josephson effects. The critical currents of the devices could be modulated by external dc magnetic fields in Fraunhofer-like patterns--expected for ideal Josephson junctions---indicating modestly uniform current densities in the junctions. The critical-current density depended exponentially with PBCO thickness yielding a normal-metal coherence length of 9 nm for this low-resistivity material and the current density could be varied over 3 orders of magnitude by varying the PBCO thickness. We observed a systematic decrease in the device operating temperature with increasing PBCO thickness. The device yield was high and the reproducibility of the device critical currents and resistances was very good.

Acknowledgments

The research described in this paper was performed by the Center for Space Microelectronics Technology, Jet Propulsion Laboratory, California Institute of Technology, and was jointly sponsored by the Defense Advanced Research Projects Agency, the Strategic Defense Initiative Organization-Innovative Science and Technology Office, and the National Aeronautics and Space Administration-Office of Aeronautics, Exploration and Technology. The authors wish to recognize many enlightening discussions with Rick LeDuc, J. Stern, A. Kleinsasser, C. Rogers, and R. Burhman.

References

- [1] K. K. Likharev, Rev. Mod. Phys. 51 (1979) 101.
- [2] S. E. Russek, D. K. Lathrop, B. H. Moeckley, R. A. Buhrman, D. H. Shin, and J. Silcox, Appl. Phys. Lett. 57 (1990) 155.
- [3] J. Mannhart, P. Chaudhari, D. Dimes, C. C. Tsuei, and T. R. McGuire, Phys. Rev. Lett. 61 (1988) 2476; D. Dimes, P. Chaudhari, J. Mannhart, and F. K. LeGoues, Phys. Rev. Lett. 61 (1988) 219.
- [4] C. L. Jia, B. Kabius, K. Urban, K. Herrmann, G. J. Cui, J. Schubert, W. Zander, A. Braginski, and Ch. Heiden, Physics C 175 (1991) 545.
- [5] D. Dimes, P. Chaudhari, J. Mannhart, and F. K. Legoues, Phys. Rev. Lett. 61 (1988) 219.
- [6] K. Char, M. S. Colclough, S. M. Garrison, N. Newman, and G. Zaharchuk, Appl. Phys. Lett. 59 (1991) 733; K. Char, M. S. Colclough, L. P. Lee, and G. Zaharchuk, Appl. Phys. Lett. 59 (1991) 2177.
- [7] P. M. Mankiewich, D. B. Schwartz, R. E. Howard, L. D. Jackel, B. L. Straughn, E. G. Burkhardt, and A. H. Dayem, in *Proceedings of the 5th International Workshop on Future Electron Devices*, Miyagi-Zao, (1988) 157.
- [8] M. G. Forrester, J. Talvacchio, J. R. Gavaler, M. Rooks, and J. Lindquist, IEEE Trans. Msg. 27 (1991) 3098.
- [9] M. S. DiIorio, S. Yoshizumi, K-Y. Yang, J. Zhang, and M. Maung, Appl. Phys. Lett. 58 (1991) 2552.
- [10] R. H. One, J. A. Bean, M. W. Cromar, T. E. Harvey, M. E. Johansson, C. D. Reintsema, and D. A. Rudman, Appl. Phys. Lett. 59 (1991) 1126.
- [11] C. T. Rogers, A. Inam, M. S. Hegde, B. Dutta, X. D. Wu, and T. Venkatesan, Appl. Phys. Lett. 55 (1989) 2032.

- [12] J. B. Barrier, C. T. Rogers, A. Inam, R. Ramesh, and S. Bersey, *Appl. Phys. Lett.* **59** (1991) 742.
- [13] J. Gao, W. A. M. Aarnink, G. J. Geritsma, and H. Rogalla, *Physics C* **171** (1990) 126; J. Gao, W. A. M. Aarnink, G. J. Geritsma, D. Veldhuis, and H. Rogalla, *IEEE Trans. Msg.* **27** (1991) 3062; J. Gao, Yu. Boguslavskij, B. B. G. Klopman, D. Terpstra, G. J. Geritsma, and H. Rogalla, *Appl. Phys. Lett.* **59** (1991) 2754; J. Gao, Yu. M. Boguslavskij, B. B. G. Klopman, D. Terpstra, R. Wijbrans, G. J. Geritsma, and H. Rogalla, *J. Appl. Phys.* **72** (1992) 575; Yu. M. Boguslavskij, J. Gao, A. J. H. M. Rijnders, D. Terpstra, G. J. Geritsma, and H. Rogalla, *Physics C* **194** (1992) 268; Yu. M. Boguslavskij, J. Gao, A. J. H. M. Rijnders, D. Terpstra, G. J. Gerritsma, and H. Rogalla, to appear in *IEEE Trans. Msg.* **29** (1993).
- [14] T. Hashimoto, M. Sagoi, Y. Mizutani, J. Yoshida, and K. Mizushima, *Proceedings of the Fourth Annual International Symposium on Superconductivity, (ISS-91)* Oct. 14-17, 1991, Tokyo, Japan; T. Hashimoto, M. Sagoi, Y. Mizutani, J. Yoshida, and K. Mizushima, *Appl. Phys. Lett.* **60** (1992) 1756; T. Hashimoto, M. Sagoi, Y. Mizutani, J. Yoshida, and K. Mizushima, to be published in *IEEE Tran. Msg.* **29** (1993).
- [15] U. Kabasawa, Y. Tarutani, A. Tsukamoto, T. Fukazawa, M. Hiratani, and K. Takagi, *Physics C* **194** (1992) 261.
- [16] B. D. Hunt, M. C. Foote, and L. J. Bajuk, *Appl. Phys. Lett.* **59** (1991) 982; B. D. Hunt, L. J. Bajuk, J. B. Barrier, M. C. Foote, B. B. Jones, and R. P. Vasquez, in *Proceedings of the SPIE Symposium "Progress in High T_c Superconducting Transistors and Other Devices"*, Sept. 12-13, 1991, San Jose, CA (*SPIE Proc. Vol. 1597*).
- [17] D. K. Chin and T. Van Duzer, *Appl. Phys. Lett.* **58** (1991) 753.

- [18] R. L. Fink, M. Thompson, C. Hilbert, and H. Kroger, *Appl. Phys. Lett.* 61 (1992) 595.
- [19] Y. Tarutani, T. Fukazawa, U. Kabasawa, A. Tsukamoto, M. Hiratani, and K. Takagi, *Appl. Phys. Lett.* 58 (1991) 2707.
- [20] M. Kasai, T. Ohno, Y. Kanke, Y. Kozono, M. Hanazono, and Y. Sugita, *Jap. J. Appl. Phys.* 29 (1992) L2219.
- [21] G. F. Virshup, M. E. Klausmeier-Brown, I. Bozovic, and J. N. Eckstein, *Appl. Phys. Lett.* 60 (1992) 2288; M. E. Klausmeier-Brown, G. F. Virshup, I. Bozovic, J. N. Eckstein, and K. S. Rails, *Appl. Phys. Lett.* 60 (1992) 2806.
- [22] R. P. Robertazzi, R. B. Laibowitz, R. H. Koch, and W. J. Gallagher, *Appl. Phys. Lett.* 61 (1992) 711.
- [23] K. Char, M. S. Colclough, T. H. Geballe, and K. E. Myers, submitted to *Appl. Phys. Lett.*
- [24] H. B. Radousky, *J. Mater. Res.* 7 (1992) 1917.
- [25] B. Fisher, G. Koren, J. Genossar, L. Patlagan, and E. L. Gartein, *Physica C* 176 (1991) 75; B. Fisher, J. Genossar, L. Patlagan, and J. Askenazi, *Phys. Rev. B* 43 (1991) 2821.
- [26] J. J. Neumeier and M. B. Maple, *Physics C* 191 (1992) 158.
- [27] R. Gross, P. Chaudhari, D. Dimes, A. Gupta, and G. Koren, *Phys. Rev. Lett.* 64 (1990) 228.
- [28] Antonio Barone and Gianfranco Paternò, *Physics and Applications of the Josephson Effect* (John Wiley & Sons, Inc., New York, 1982), Chap. 4.
- [29] Peter A. Rosenthal, M. R. Beasley, K. Char, M. S. Colclough, and G. Zaharchuk, *Appl. Phys. Lett.* 59 (1991) 3482.

Figure Captions

Figure 1. Shown here is a cross-sectional schematic of our edge-geometry all-high- T_c SNS device. The edge fabrication is by Ar-ion milling using the MgO mask and followed by the deposition of the $\text{PrBa}_2\text{Cu}_3\text{O}_{7-\delta}$ (PBCO) and $\text{YBa}_2\text{Cu}_3\text{O}_{7-\delta}$ (YBCO) films in situ. The orientation of the YBCO and PBCO films is with the c-axis normal to the LaAlO_3 substrate surface. The deposition of the YBCO and PBCO films is by laser ablation. The current path through the device is shown in the schematic.

Figure 2. This is a cross-sectional transmission electron micrograph of PBCO/YBCO/Au trilayer on a LaAlO_3 substrate. The sequential in situ deposition of these films took place during the barrier-counter electrode deposition step of the SNS device fabrication. The PBCO, YBCO and Au thicknesses were approximately 50, 200 and 30 nm, respectively. Overall, there is good layering and coverage of the oxides. However, there is a roughness in the films of about 6 to 7 nm

Figure 3.” Plotted here is the average PBCO resistivity as a function of temperature. The determination of the resistivity for the c-axis oriented films was by lateral transport as shown in the inset. The value of the resistivity is several orders of magnitude lower than previously reported for bulk, granular PBCO.

Figure 4. Plotted are the low-current resistances of our YBCO/PBCO/YBCO edge-geometry devices as a function of temperature for the three different PBCO thicknesses indicated. The inset is a scale expansion of the plot that makes clear that the $R(T)$ foot depends on the PBCO thickness. Note that measurement of the counter- and base-electrode transition temperatures indicated they are between 85 and 88 K for all three devices.

Figure 5. We show here a typical current-versus-voltage (I-V) characteristic for a device with a 10 rim-thick PBCO barrier layer. Overall, the curvature of the I-V is consistent with the resistively-shunted-junction model. The temperature was 65 K. (100 μ V horizontal scale, 200 μ A vertical scale).

Figure 6. This is the I-V characteristic for the device of Fig. 5 but with the device under 10.5 GHz microwave irradiation. As can be *seen*, the I-V exhibits strong Shapiro steps expected for an SNS Josephson junction with low-capacitance. The temperature was 65 K. (20 μ V horizontal scale, 50 μ A vertical scale).

Figure 7. The critical current (.) of a YBCO/PBCO/YBCO device plotted as a function of an applied dc magnetic field. There is an overall $\sin(x)/x$ -like response (dashed line) observed and expected for an Josephson junction with a uniform current distribution within the junction. However, the critical current does not modulate fully to zero suggesting there is some non-uniformity in the barrier.

Figure 8. Plotted here is the critical current and inverse resistance versus device area for a chip at 4.2 K with a 10 rim-thick PBCO layer. Observed is the expected areal scaling for these parameters.

Figure 9. The critical-current density plotted as a function of PBCO thickness for data taken at 4.2 K. The data exhibit the expected exponential dependence. A fit to the data reveals a coherence length of 9 nm for the PBCO.

Figure 10. This is a plot of the device resistances as a function of PBCO thickness for data taken at 4.2 K. Observed is the linear dependence of the resistance on PBCO thickness. A fit to the data reveals an average resistivity of \cdot 30 m Ω cm for the PBCO as determined from the YBCO/PBCO/YBCO edge-geometry

devices. This value is consistent the results obtained from lateral transport through an individual PBCO film (see figure 3).

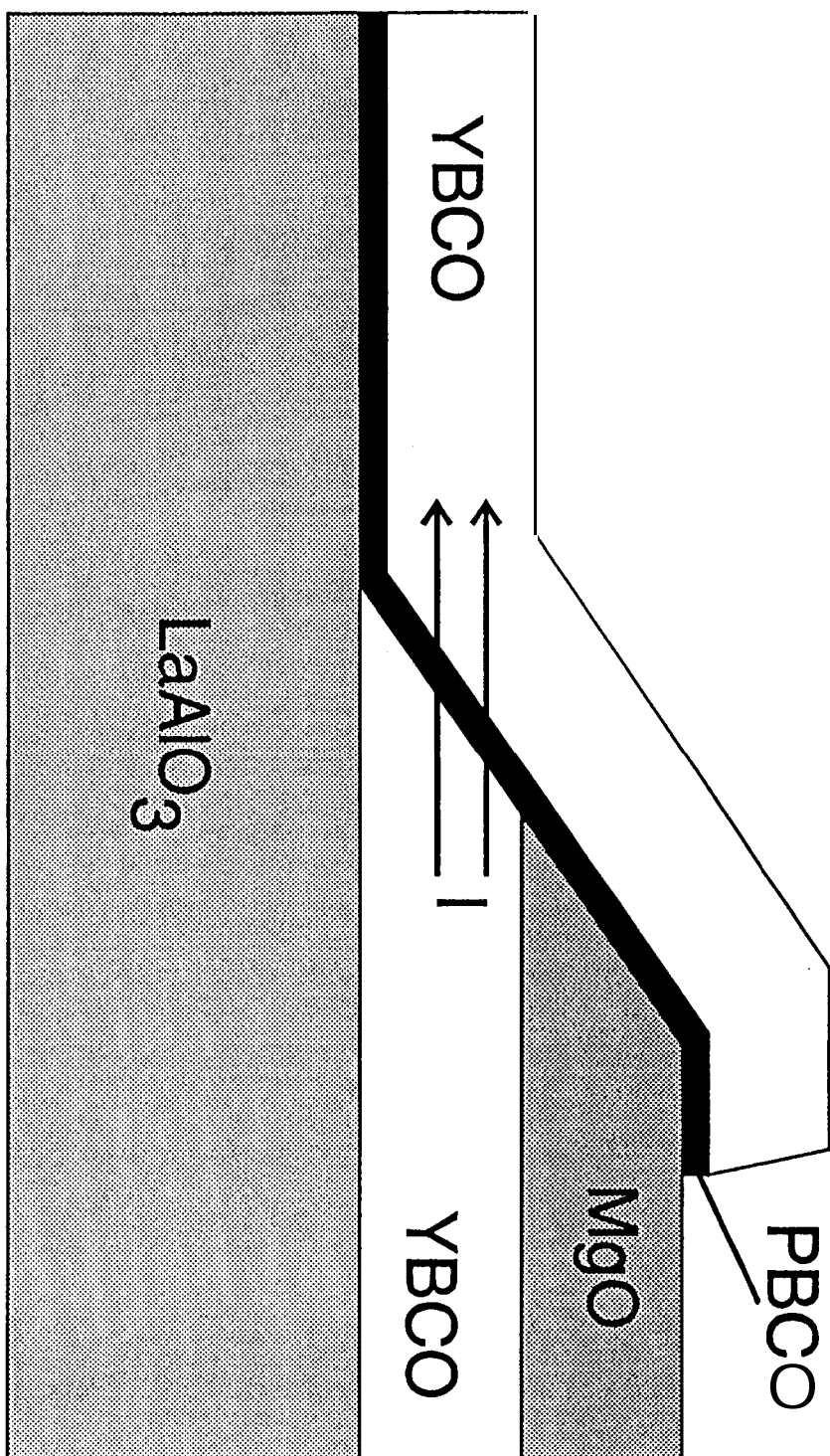


Figure 1.

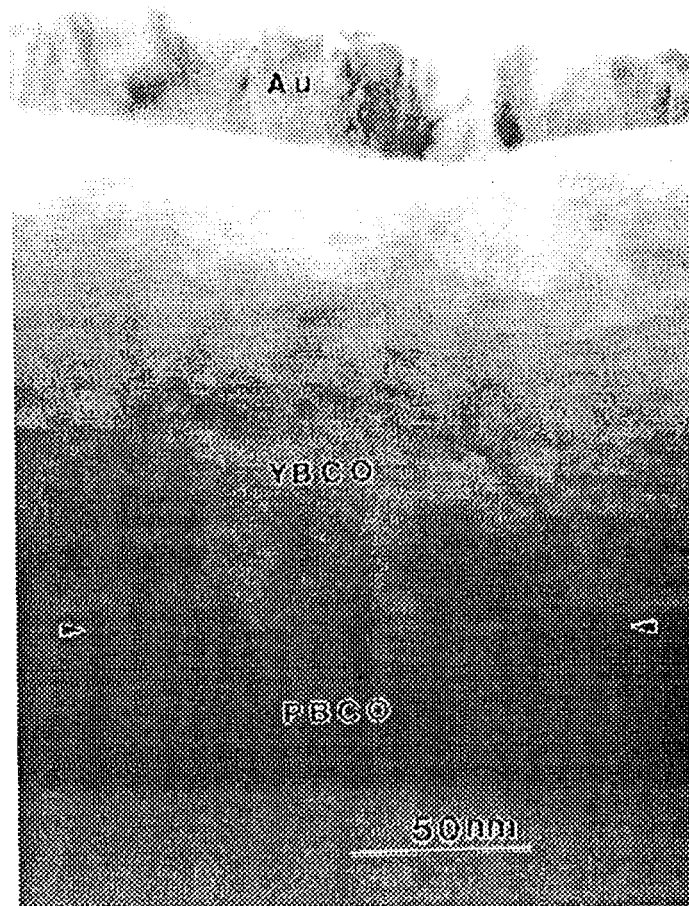


Figure 2.

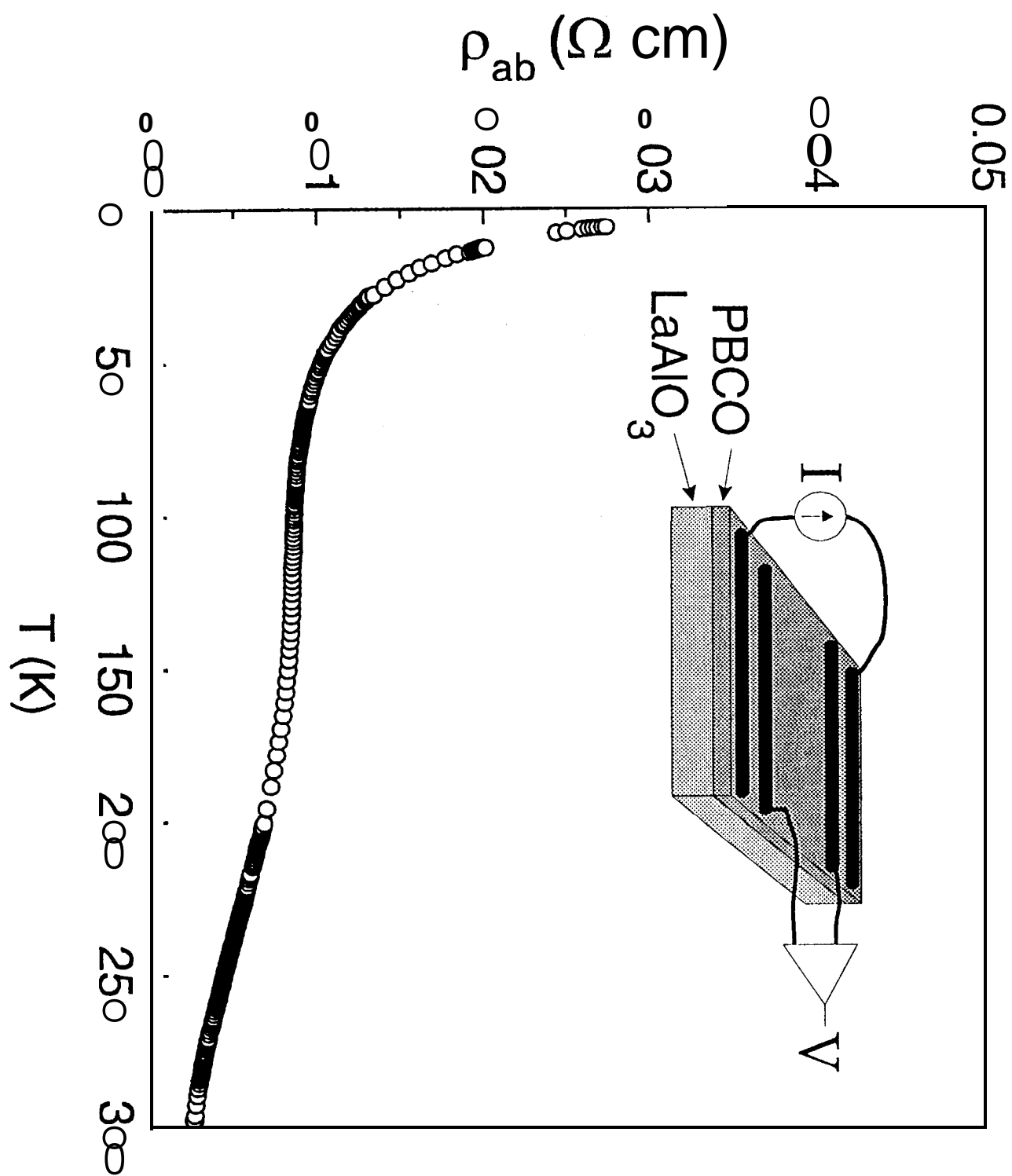


Figure 3.

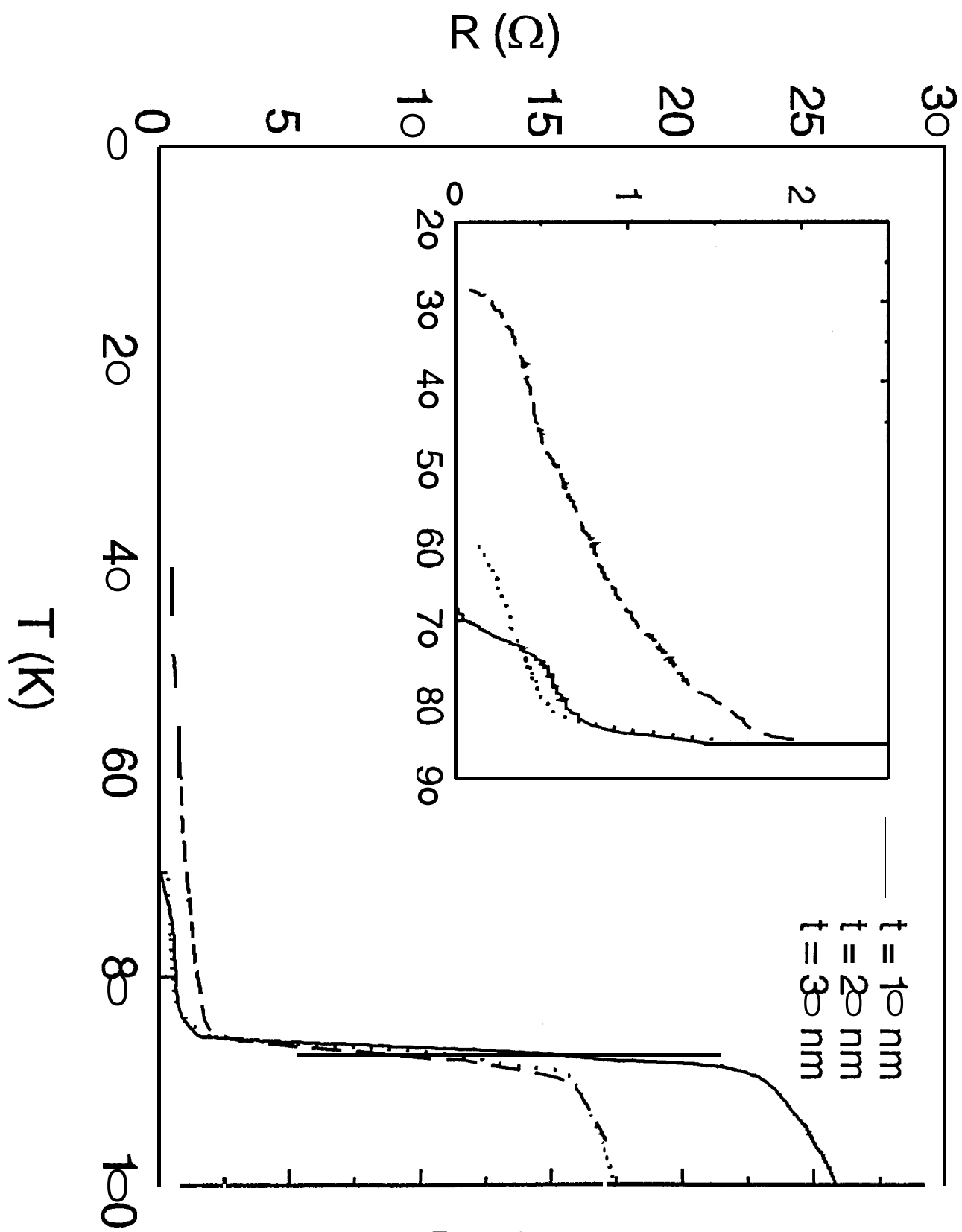


Figure 4.

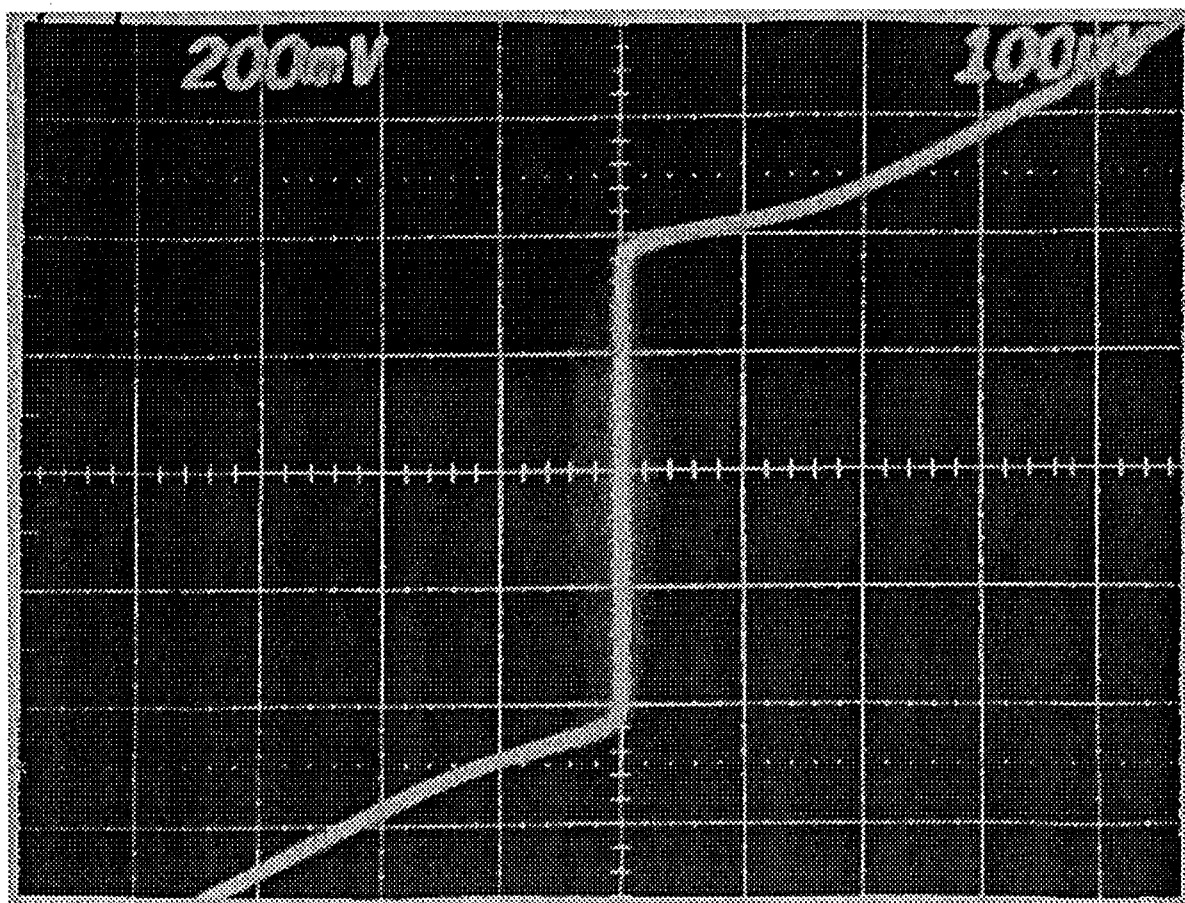


Figure 5.

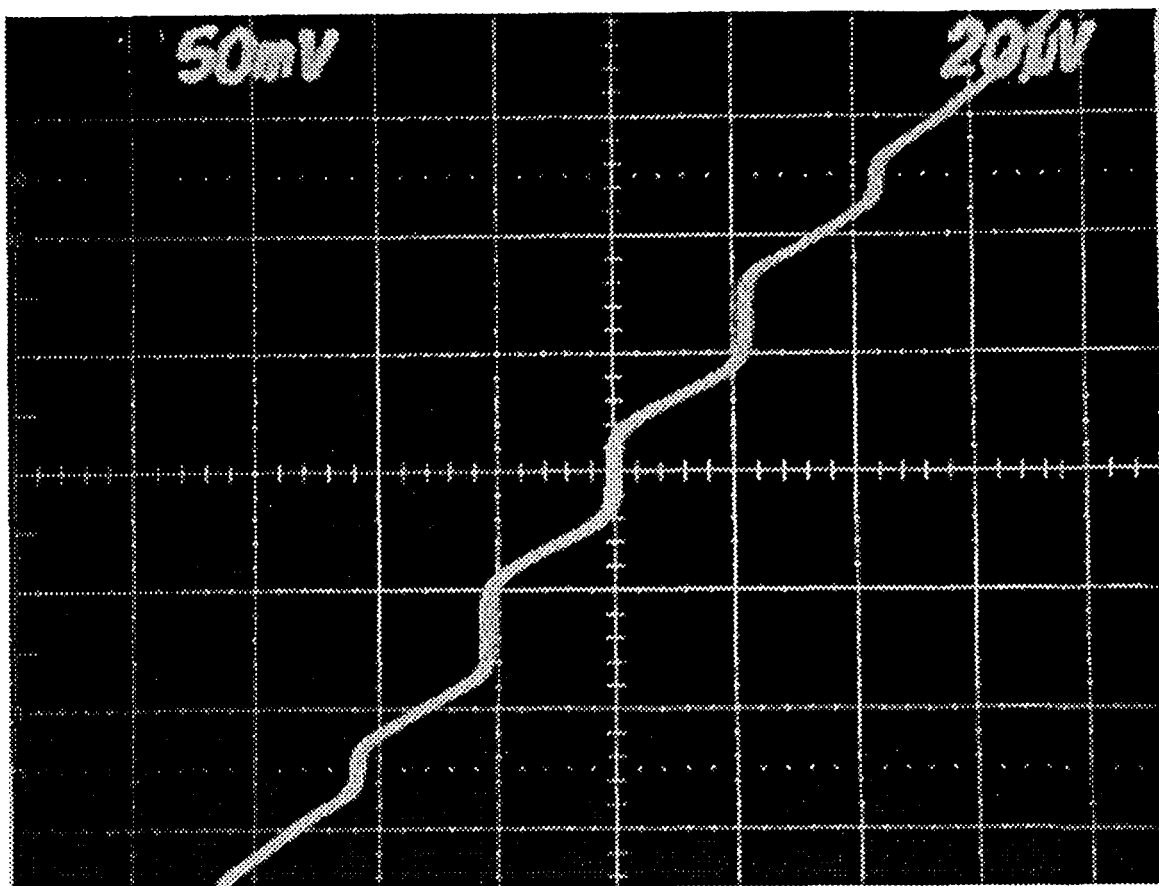


Figure 6.

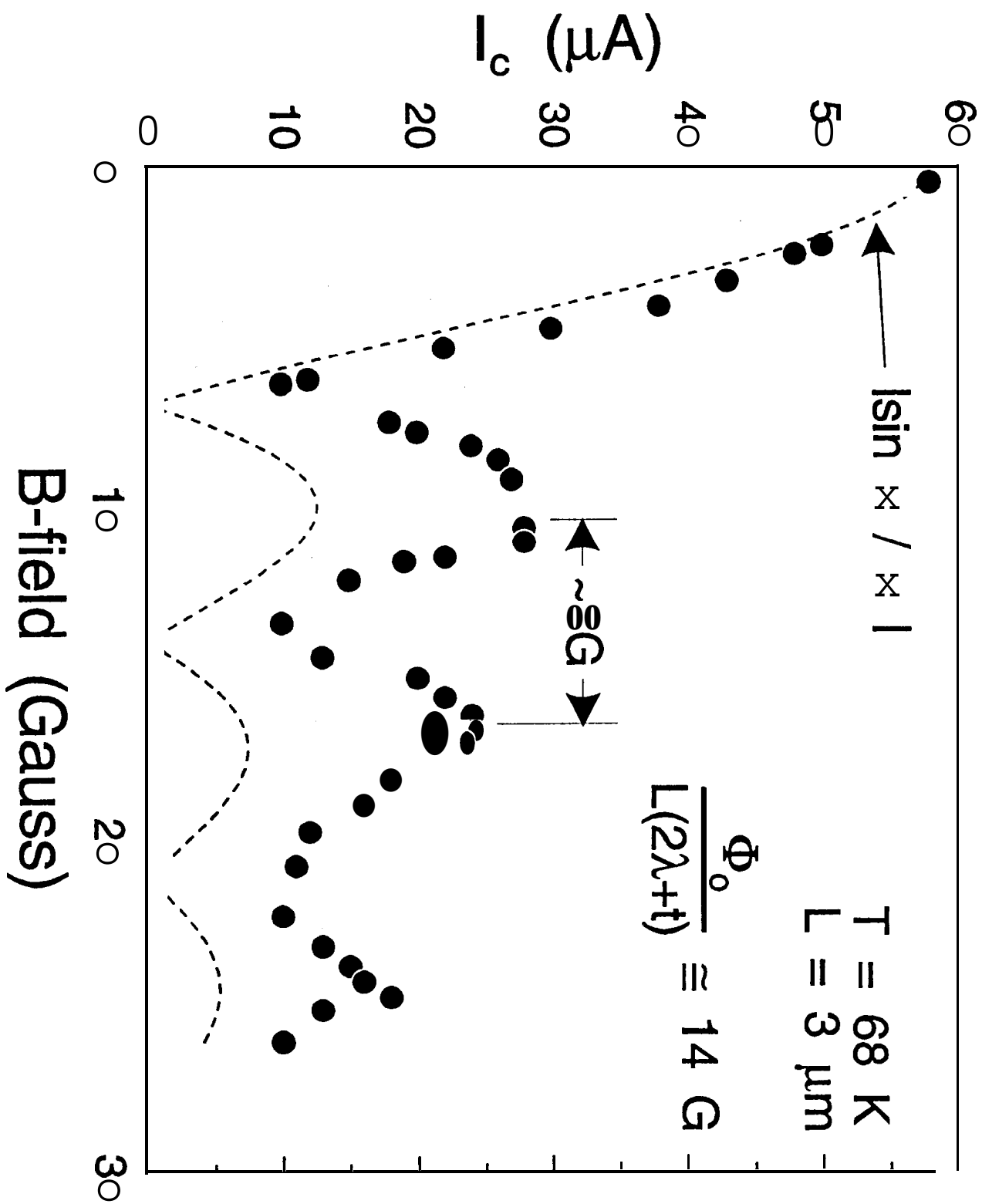


Figure 7.

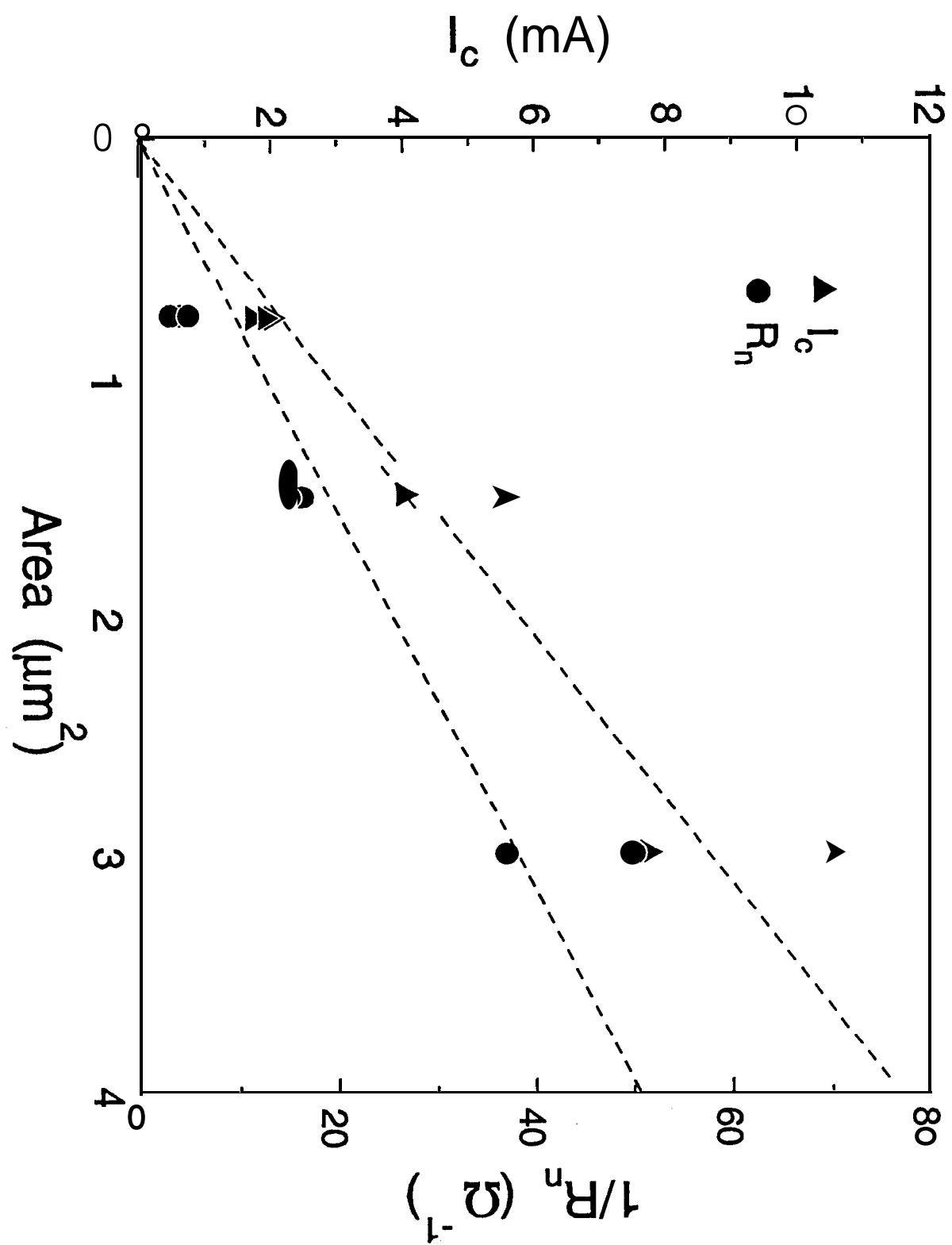


Figure 8.

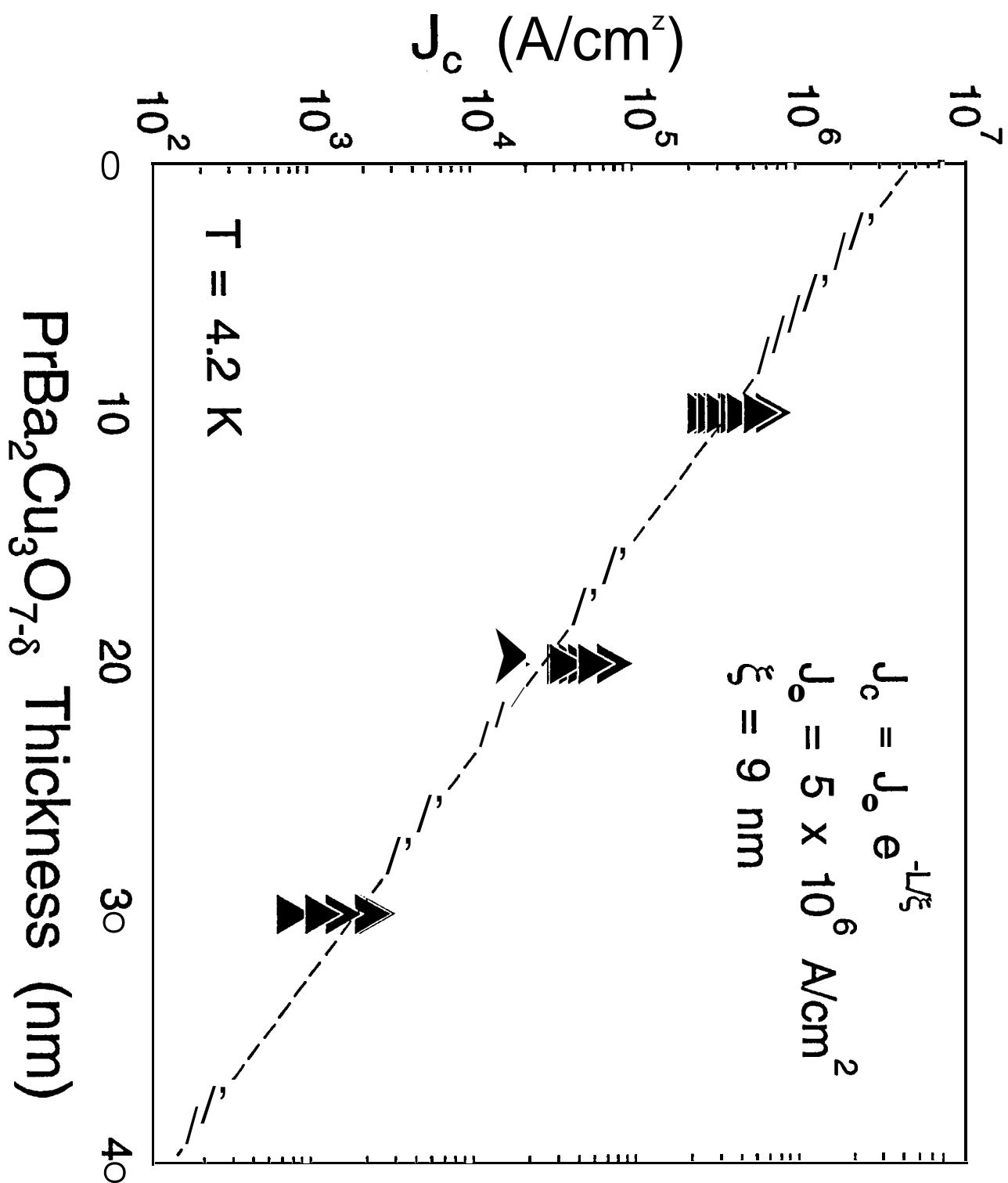


Figure 9.

